nature geoscience

REVIEW ARTICLE

PUBLISHED ONLINE: 20 JUNE 2016 | DOI: 10.1038/NGEO2733

Continent-sized anomalous zones with low seismic velocity at the base of Earth's mantle

Edward J. Garnero*, Allen K. McNamara and Sang-Heon Shim

Seismic images of Earth's interior reveal two massive anomalous zones at the base of the mantle, above the core, where seismic waves travel slowly. The mantle materials that surround these anomalous regions are thought to be composed of cooler rocks associated with downward advection of former oceanic tectonic plates. However, the origin and composition of the anomalous provinces is uncertain. These zones have long been depicted as warmer-than-average mantle materials related to convective upwelling. Yet, they may also be chemically distinct from the surrounding mantle, and potentially partly composed of subducted or primordial material, and have therefore been termed thermochemical piles. From seismic, geochemical and mineral physics data, the emerging view is that these thermochemical piles appear denser than the surrounding mantle materials, are dynamically stable and long-lived, and are shaped by larger-scale mantle flow. Whether remnants of a primordial layer or later accumulations of more-dense materials, the composition of the piles is modified over time by stirring and by chemical reactions with material from the surrounding mantle, underlying core and potentially from volatile elements transported into the deep Earth by subducted plates. Upwelling mantle plumes may originate from the thermochemical piles, so the unusual chemical composition of the piles could be the source of distinct trace-element signatures observed in hotspot lavas.

The movement of Earth's tectonic plates, which includes divergence at mid-ocean ridges to create new crust and lithosphere, as well as convergence and consumption of older plates into Earth's interior at subduction zones, is related to convective motions of the underlying mantle rock over geologic timescales. The mantle, which extends to about 2,900 km depth, just less than halfway to Earth's centre (near 6,400 km), actively convects because it is heated from below, by the hot liquid outer core, as well as from within due to radioactive decay of uranium, thorium and potassium. This transport of heat involves advection and stirs the mantle.

The locations of current and past tectonic plate subduction zones at Earth's surface overlie seismically imaged, or tomographically observed, regions with higher-than-average seismic wave speeds in the deepest mantle. This spatial correlation is consistent with the expectation of descending former lithosphere being cooler and therefore denser than the surrounding mantle. Away from those locations are regions with lower-than-average wave speeds in the deepest mantle. To first order, these regions largely underlie surface locations of hotspot volcanism[1]. This correlation, combined with tomographic imaging of subducting lithosphere descending into the lower mantle in some places, has led to greater acceptance that whole mantle convection is occurring. The lowered wave speeds in global shear wave velocity (V_S) tomography models occur in two, nearly-antipodal, large low shear velocity provinces (LLSVPs; Fig. 1a): one is centred beneath the Pacific Ocean and the other is located beneath the Atlantic Ocean and the western and southern part of the African continent. The large-scale shape of the LLSVPs, as inferred from tomographic models from different research groups[2] (Supplementary Fig. S1), is in general agreement, although differences are present at short scales (Supplementary Fig. S2).

Character of LLSVPs

When decomposed into spherical harmonics, seismic tomography demonstrates that the LLSVPs are strongly characterized by degree two structure, in addition to a lesser but significant degree three contribution[1,3,4]. The strongest lateral gradients in V_S perturbations occur at LLSVP boundaries (Fig. 1b). The detailed nature of LLSVP margins in the lowermost 200 km of the mantle varies from model to model (Fig. 1c; see also Supplementary Information).

The vertical extent of reduced LLSVP velocities between models is similarly divergent, but extends as far up as 1,200 km above the core–mantle boundary (CMB) in places[5–8]. Models consistently reveal different shapes for the Pacific and African LLSVPs: the Pacific LLSVP has a relatively round shape whereas the African LLSVP is more elongated in the north–south direction in the north and stretched eastward in the southernmost part.

A number of high-resolution, forward modelling seismic studies have shown that shear waves travelling in the deep mantle near LLSVP edges become broadened and/or shifted in time[2,5,9–11]. This is consistent with a phenomenon called multi-pathing, where a seismic wave incident on strong heterogeneity can parse into energy that travels through the heterogeneity, as well as energy that refracts around it. The different waves travel at different speeds, thus resulting in either a broadened pulse or even two distinct pulses. The locations of the imaged sharp boundaries roughly coincide with LLSVP edges seen in tomography (Fig. 1d; see also Supplementary Fig. S3). This roughly corresponds to LLSVPs occupying an area of 30% of the CMB. Waveform studies also indicate that the tops of both LLSVPs may be sharp in some places[2,5,9,10].

Tomographic models suggest significant heterogeneity within LLSVPs (Supplementary Fig. S1, right column). Within the LLSVP regions, forward modelling seismic studies have identified heterogeneities at scales much smaller than tomography can resolve. For example, isolated structures at scales from hundreds of km to 1,000 km in the lateral dimension have been mapped at the base of the mantle within the Pacific LLSVP[5]. At even shorter scales, forward modelling studies find thin patches with strong wave speed reductions right above the CMB, called ultralow

School of Earth and Space Exploration, Arizona State University, Tempe, Arizona 85287-6004, USA. *e-mail: garnero@asu.edu

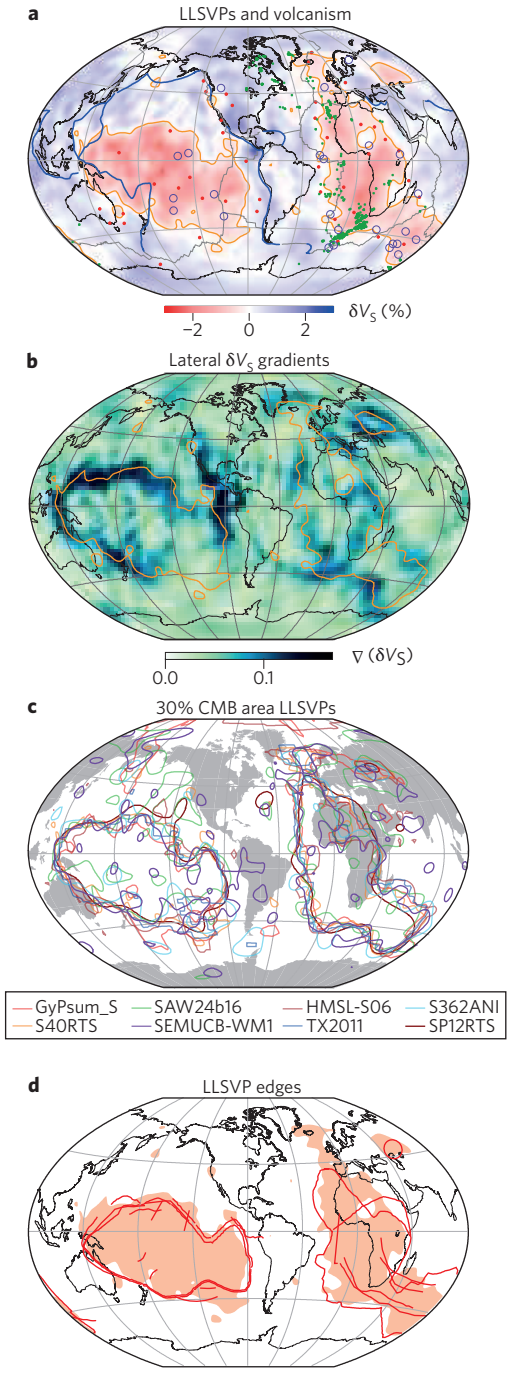

Figure 1 | Large low shear velocity provinces (LLSVPs) with other phenomena. a, Lowermost mantle shear velocity perturbations (δV_S) are shown for model S40RTS (ref. 1) at depth (*z*) of 2,800 km. Blue and red shading corresponds to positive and negative δV_S, respectively. The thick orange line at $\delta V_S = -0.27\%$ highlights LLSVP structure corresponding to 30% of the core–mantle boundary (CMB) area. Convergent margins (blue lines) overlay high δV_S. Surface hotspots (red dots), large igneous province origination locations (purple circles[6]) and some kimberlites (green dots[34]) overlay low δV_S, especially LLSVP margins. **b**, Strong lateral gradients (∇) in δV_S are shown (darker colours are strongest), which match well with the LLSVP contour of **a**. **c**, The 30% area LLSVPs of eight models, represented by eight coloured lines as detailed in the key (Supplementary Fig. S1 displays original models). **d**, The 30% area LLSVP of S40RTS is shaded orange, and shown with red lines corresponding to forward modelling studies that map sharp LLSVP edges, which to first order are near LLSVP margins seen in tomography (more detail is given in Supplementary Fig. S3).

velocity zones (ULVZs); ULVZs are commonly mapped within and near the margins of LLSVPs[12]. ULVZ thicknesses vary, but are commonly between 5 and 20 km. Additional smaller-scale deep mantle heterogeneity (1–10 km) has been advocated from scattering studies[13], with some evidence for increased scattering near LLSVP margins[14].

A form of intermediate-scale heterogeneity within LLSVPs includes horizontal layering interpreted as due to a phase change into, and then out of, the stability field of a higher-pressure polymorph (post-perovskite) of the most abundant lower mantle mineral, bridgmanite[15], which can affect seismic observations as well as dyanmics[16,17]. In the Pacific LLSVP, this has been interpreted as a lens of post-perovskite in compositionally distinct material, because the double-crossing of the post-perovskite phase transition is unlikely in higher-temperature regions of pyrolitic mantle[18] (though it is important to note that the deepest mantle temperature is not well constrained). Numerical convection calculations have shown that subducted oceanic crust is expected to become incorporated into thermochemical piles[19–21]. This basaltic material contains bridgmanite and free silica, which individually undergo phase transitions (to post-perovskite and to seifertite, respectively) at different lowermost depths[22,23], and therefore, may contribute to a cause of the seismic wave reflections.

Seismic wave speed anisotropy has also been documented to exist within and near LLSVPs (for example, Fig. 2a) from increased shear wave splitting seen in SKS or SKKS waves that exit the core and travel up along the LLSVP sides[24,25]. If LLSVPs are indeed thermochemical piles, the convective flow that shapes the piles may serve to increase strain along pile margins. This may result in preferential alignment of compositional heterogeneity (for example, stretched blebs of pile material and/or former oceanic basaltic crust, or stretched pockets of partial melt associated with ULVZ material) and/or lattice-preferred orientation in these zones, giving rise to the observed shear wave splitting near LLSVP margins.

At present, the degree of correlation between lowermost mantle P-wave velocity heterogeneity (δV_P) and δV_S in LLSVP regions varies between models. Comparisons of δV_S and δV_P models show qualitative agreement between LLSVPs and large low δV_P zones, but the small-to-intermediate-scale structure differs strongly (to different degrees in different models; Supplementary Fig. S4). Some forward modelling analyses suggest that the edges of the Pacific LLSVP agree with large low δV_P zones that explain P-wave core-phase travel times[11]. If some regions exhibit disagreement between lower mantle δV_S and δV_P structure, a mechanism that affects V_P differently from V_S is required to explain the disagreement, such as the post-perovskite phase transition, anisotropy or distinct composition[4]. Since the low velocity provinces are present for both P and S waves, hereafter we refer to them generally as large low velocity provinces (LLVPs), unless there is need to specifically point to LLSVPs (that is, the shear velocity provinces).

Early suggestion of elevated density in LLVPs came from normal mode studies[26], but the sensitivity of modes to density is much lower than their sensitivity to seismic velocities, and thus density is less resolved[27,28]. Simultaneous determination of both lowermost mantle V_P and V_S is required[4]. An increase in amplitude of δV_S heterogeneity relative to δV_P (ref. 29) and the anti-correlation between shear and bulk sound velocity ($[V_P^2 - 4/3V_S^2]^{1/2}$) heterogeneity in the lower mantle[4,30] are consistent with a thermochemical origin to LLVPs. While reduced resolution of density as well as differing ray path coverage of deep mantle by P and S waves adds difficulty in constraining this pattern, the addition of deep mantle sensitive Stoneley mode data in recent joint P and S wave inversions supports a reduction in LLVP density greater than 100 km or so above the CMB[31]. This is consistent with large-scale thermal upwelling, but does not rule out stable thermochemical

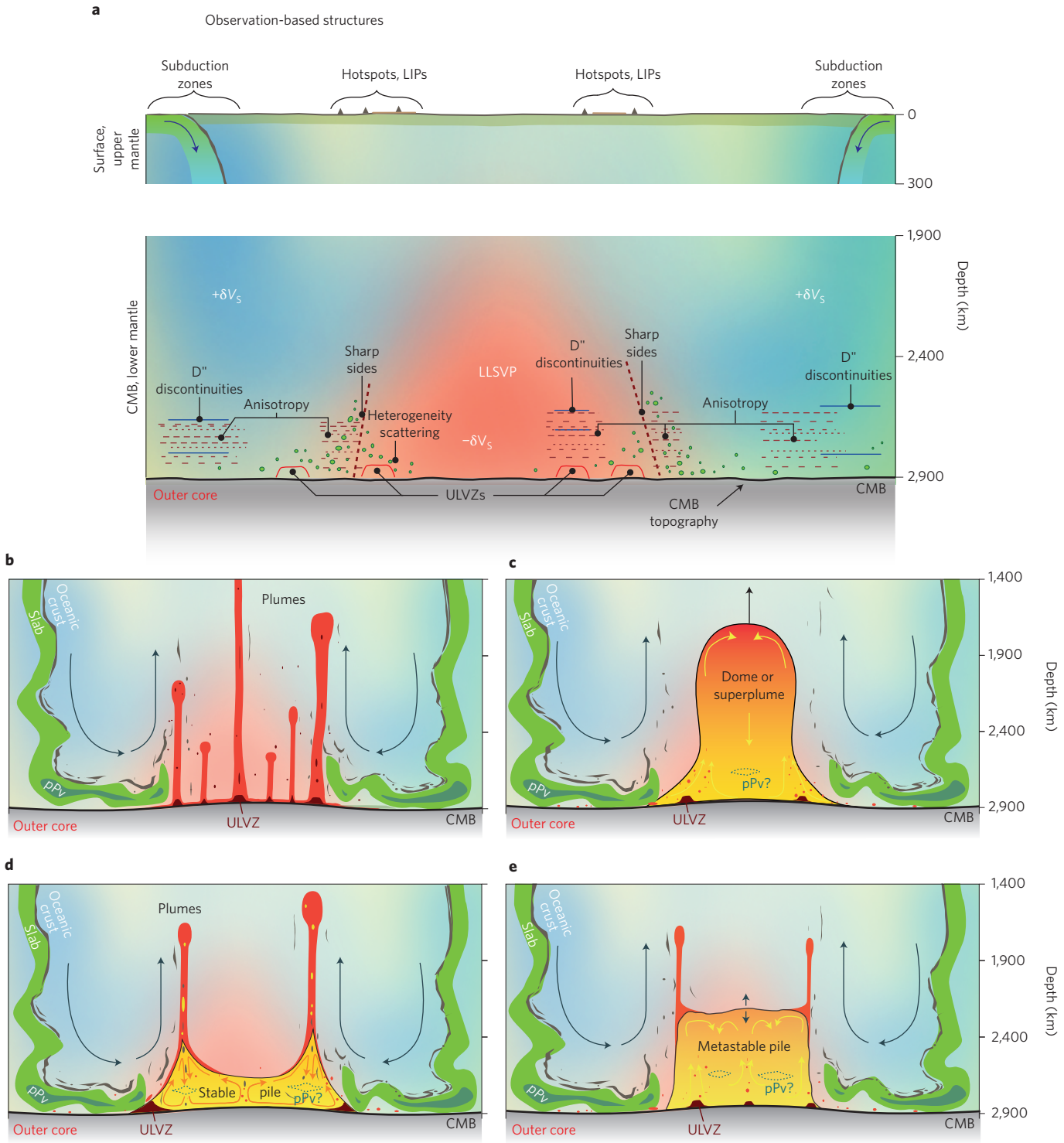

Figure 2 | LLSVP observations and interpretations. a, Surface features (upper panel) and seismically determined lower-mantle phenomena (lower panel). See text for details. **b**–**e**, Idealized possibilities proposed to explain LLSVPs. In all cases, subducted material (possibly including post-perovskite, pPv) surrounds the structure of interest that maps as the LLSVP. **b**, Plume cluster. **c**, Thermochemical superplume. **d**, Stable thermochemical pile. **e**, Metastable thermochemical pile. LIPs, large igneous provinces; CMB, core–mantle boundary; ULVZs, ultralow velocity zones.

piles, since piles can still have higher density than the mantle above LLVPs, yet lower than surrounding downwelling regions having greater negative buoyancy. In the lowest 100 km of the mantle, piles may have elevated density compared with the surrounding mantle[31], which does not preclude upwelling components to the thermochemical structures[8].

Correlations with surface features

Present-day LLVP locations exhibit geographical relationships with several phenomena observed at Earth's surface (Fig. 1a). For example, the present-day locations of convergent tectonic plate margins overlie higher-than-average lowermost mantle shear velocities, and hence, to first order, do not overlie LLSVPs. Thus, LLSVP

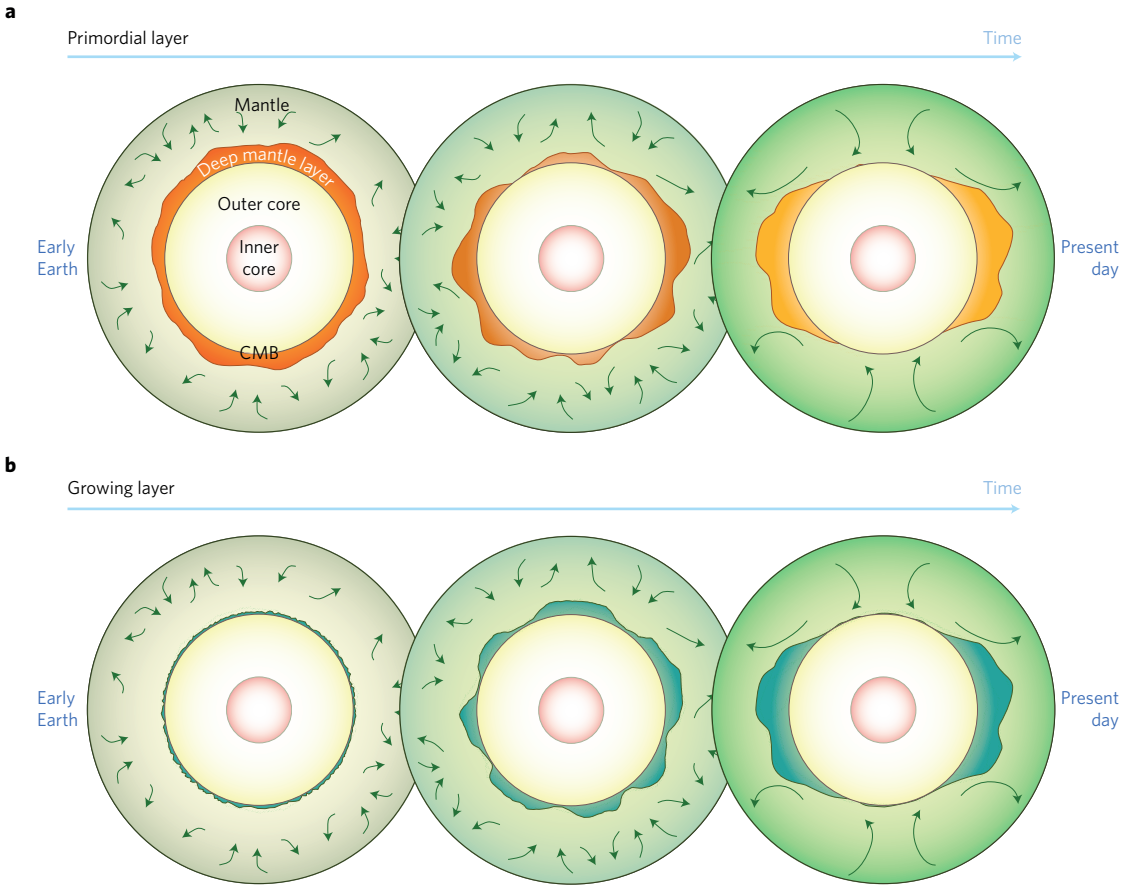

Figure 3 | Thermochemical pile evolution. Two end-member evolutionary pathways for a present-day thermochemical pile are illustrated. **a**, Primordial layer: in this scenario, early Earth processes establish a global layer, which develops into separate piles over time. **b**, Growth of the thermochemical layer over time: here, material with elevated density collects at the core–mantle boundary over time, which grows into a thicker layer and eventually into distinct thermochemical piles.

locations appear uncorrelated, or even anti-correlated, to subduction. Hotspot volcanism, on the other hand, more commonly overlies LLSVP regions. Additionally, hotspots are more likely to overlie the strongest lateral gradients at the base of the mantle than the lowest[32,33]. The strongest lateral gradients coincide with LLSVP edges (Supplementary Fig. S5), which implies hotspots more commonly overlie LLSVP edges than their interior. Recent tomographic work suggests broad conduits of reduced wave speeds beneath some hotspots, extending from the CMB up to ~1,000 km depth[8].

Earth's largest volcanic eruptions are infrequent, massive flood basalt events, resulting in large igneous provinces (LIPs). Evidence for roughly two dozen of these is preserved, and after their locations of origin are computed (which requires tectonic plate reconstruction), their past surface locations strongly correlate with present-day LLSVP edges in the deepest mantle[32,34] (Fig. 1a). The origination locations of many continental kimberlites also show good correlation with the African LLSVP[34]. While uncertainties in plate reconstruction as well as LLSVP shape (for example, round versus elongated) and fixity of location may affect some measures of correlation[35], the evidence is compelling that these different forms of intraplate eruptions correlate with the present-day locations of LLSVPs, and in particular their margins. Furthermore, numerical calculations demonstrate the feasibility of thermal plumes to form near thermochemical pile margins[36].

Some hotspots have parallel tracks of volcanoes with each track possessing distinct isotopic ratios of trace elements[37,38]. This phenomenon has been attributed to zoning in plumes in which the plume root is at the edge of compositionally distinct lowermost mantle reservoir: LLVPs are proposed to be reservoirs that are dominantly entrained into one side of the plume, whereas surrounding mantle materials dominate the other side of the plume[39]. A challenge with this hypothesis regards how to map geographic patterns of isotope ratios in surface lavas directly to similar geographic patterns of mantle source heterogeneities.

Relationship to deep mantle convection

Seismic studies continue to improve resolution of present-day LLVP structure and the surrounding deep mantle (Fig. 2a), providing motivation for understanding their origin, evolution and underlying dynamics. The observation that LLVPs are located away from subduction and underlie the majority of hotspots is consistent with mantle convection studies that employ plate history as a surface velocity boundary condition. This imposed surface flow guides the locations of subduction, resulting in slab-driven convective downwelling. At the CMB, this convective flow spreads laterally away from downwelling zones and pushes dense material into piles, generating large-scale return-flow upwelling in LLSVP regions[40–42]. A key question is whether LLVPs are hot thermal upwelling anomalies in an effectively isochemical lower mantle, or whether they are piles of intrinsically more-dense mantle material that have accumulated at the base of large-scale, global upwelling regions. If LLVPs are intrinsically more-dense piles, critical questions include how did they form, what are they composed of, how long have they existed and are they dynamically stable over geologic timescales (as well as, how do dense piles account for a seismic velocity reduction)?

An early interpretation of LLVPs was that they are caused by large thermal megaplumes[43]; however, for conventional material parameters and Earth-like convective vigour, mantle convection studies predict individual mantle plumes to be much smaller in the lateral dimension than the LLVPs[41,44]. An alternative possibility in an isochemical lower mantle is that the LLVPs are poorly imaged clusters of thermal mantle plumes (Fig. 2b) that resemble larger structures when viewed through the blurred lens of tomography[41,44]. While it has been shown that seismic tomography should indeed blur clusters of thermal plumes[41,45], there is debate whether thermal anomalies alone can satisfactorily explain the strong low-wavelength character of LLVPs[41,45,46].

The strong lateral gradients in shear wave speed observed along LLSVP margins (Supplementary Fig. S5) can be explained by the low velocity provinces being compositionally distinct from the surrounding mantle. Geodynamical studies have found that only a small increase in intrinsic density (up to a few per cent) is required for material to form into lowermost piles on similar spatial scales as LLVPs[40,41,47–49]. Two contrasting end-member explanations exist for their origin: they are remnants of a global layer from very early Earth or they are growing over time (Fig. 3). Piles formed early in Earth's history may be the remnants of an ancient differentiation event or process[50–53], and can be considered primordial thermochemical piles. These are expected to have sharp compositional boundaries, which limit heat and chemical exchange with the surrounding mantle. On the other hand, piles may have been continuously forming from the early Earth to the present day, for example, by the accumulation of subducted oceanic crust[20,48,49,54], or chemical reactions between the mantle and core[55,56]. One complication for the oceanic crust hypothesis is that it is difficult to accumulate intrinsically more-dense crust of present-day thickness (6 km) at the CMB because viscous stresses from mantle convection act to stir it into the background mantle[57]. However, if oceanic crust was denser or thicker in the past, it could have more easily accumulated into piles[20,48]. Additionally, if the location of subduction does not change over time, recent geodynamical work demonstrates that oceanic crust of present-day thickness can indeed accumulate at the CMB, forming piles[49].

If the origin of LLVPs is primordial thermochemical piles, their intrinsic density difference with the background mantle will control their vertical stability. For relatively low-density contrasts between piles and surrounding mantle, piles may form domes (Fig. 2c) that vertically rise (and depending on density, sink) throughout the mantle[58]. However, it is unclear whether such structures can be stable for geologic timescales without being stirred into the background mantle. These structures are commonly called domes or superplumes. For larger-density contrasts, negatively buoyant piles are expected to remain in the lowermost mantle and persist over geologic timescales[47] (Fig. 2d). If thermochemical pile material has a bulk modulus that is different from background mantle, its density can have a different pressure dependence than the surrounding mantle, leading to a depth-dependent density contrast. This may lead to metastable piles (Fig. 2e), with their deeper portions being more buoyant than their upper portions, producing more-upright structures with steep sides[59].

Geodynamic studies that impose historical plate motions as a surface boundary condition in spherical mantle convection produce piles that are geographically located in seismically determined LLVP regions, with shapes similar to that observed in seismic tomography[3,40–42,60]. For piles to remain in the lowermost mantle, they must, on average, be more negatively buoyant than the surrounding mantle rock they displace. For a thermochemical layer to be swept away from downwelling slab regions to form piles, they must generally be less negatively buoyant than the slab material that displaces them. This is supported by geodynamical studies that examine the radial stresses imposed on the CMB interface from thermochemical convection[60], as well as supported by the recent normal mode work[4]. The geodynamic studies predict that the CMB is most depressed beneath subduction regions and relatively flat and less depressed (or even slightly uplifted) beneath pile regions. However, constraining CMB topography from seismology is difficult due to the trade-off between unmapped deep mantle heterogeneity and CMB topography; this is punctuated by poor agreement between CMB topography models[60]. However, recent investigations suggest joint seismic–geodynamic inversions help to explain normal mode data sensitive to CMB topography, and are consistent with geodynamic predictions of thermochemical piles[61].

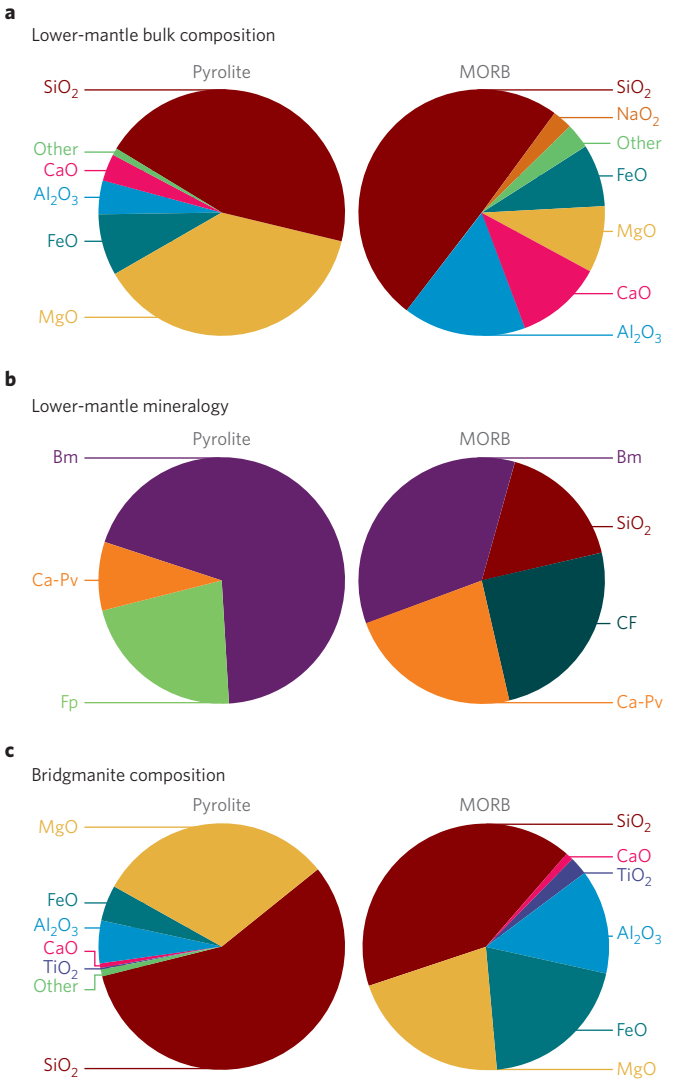

Figure 4 | Chemical composition and mineralogy of pyrolite versus mid-ocean ridge basalt (MORB). a, Bulk chemical compositions of pyrolite[97] and MORB[98]. **b**, Mineralogy of pyrolite[99] and MORB[22,100] in the lower mantle. **c**, Chemical compositions of bridgmanite in pyrolite[99] and MORB[100] compositions. Bm, bridgmanite; Fp, ferropericlase; Ca-Pv, $CaSiO_3$ perovskite; CF, Ca-ferrite-type phase. All proportions are given in weight%.

Geodynamical calculations reveal that plume instabilities occur off cusps or ridges formed at the tops of piles, with the proximity to pile margins depending on pile morphology, which in turn depends strongly on rheological and density differences between the pile and surrounding mantle[59]. Any thermal instabilities formed at the CMB outside of thermochemical pile regions are subject to the same lateral flow that shapes the piles, and thus are expected to be swept towards pile locations.

Compositional evolution of deep mantle

Models invoking solely a thermal origin to lowermost mantle heterogeneity can predict some characteristics of the seismic properties

Table 1 | Summary of LLVP observations, models and interpretations.

Phenomena	Description	Interpretations	Comments
LLVP sharp margins	Seismic observation: LLVP margins have strong lateral δV_S gradients or 'edges' (Fig. 1 and Supplementary Figs S1 and S3).	LLVPs are compositionally distinct.	The degree of sharpness variable among studies and methods.
LLVP sharp tops	LLVP tops are sharp in places[5,9,10].	LLVPs are compositionally distinct.	Not well studied.
LLVP density	Seismic inference: LLVPs have been imaged with slightly elevated[26], and more recently, reduced[31] density than surrounding mantle.	LLVPs are compositionally distinct from surrounding lower mantle (high density). LLVPs are thermal upwellings (low density).	Density is difficult to constrain. Piles may have intrinsically higher density than the mantle they displace, but imaged with lower density than surrounding colder subduction-related downwelling.
LLVP seismic anisotropy	Seismic observation: seismic anisotropy is detected near LLVP margins[24,25].	Convection along pile margins may produce lattice- or shape-preferred orientation.	Not well studied.
ULVZs in or near LLVPs	Seismic observation: ULVZs commonly within LLVPs or near their margins[12].	ULVZs may be partially molten, and related to highest mantle temperatures near pile margins.	ULVZ distribution is not well constrained globally. Some ULVZs mapped far from LLVPs. There may be more than one type of ULVZ.
Seismic wave scattering	Seismic observation: increased small-scale heterogeneity has been imaged close to LLVP margins[14].	LLVPs are thermochemical piles, and may collect heterogeneities near margins.	Not well studied.
Anti-correlated wave speeds	Seismic observation: joint P and S tomographic studies suggest shear and bulk sound speeds are anti-correlated in places (Supplementary Fig. S4).	Compositional heterogeneity is present.	P and S coverage in the deep mantle differ, and are non-uniform. Post-perovskite may affect V_P differently from V_S.
Hotspot locations	Correlation analysis: many hotspots and large igneous province origination locations overlay LLVP margins[32–34].	Whole mantle plumes are generated near thermochemical pile margins[36].	This implies minimal deflection of plumes responsible for hotspots and LIPs. Older LIPs mapping over LLSVP edges suggests stability of piles for (at least) the recent past.
Hotspot geochemistry	Geochemical observation: hotspots contain distinct isotope ratios of trace elements compared with mid-ocean ridge basalts[93].	Whole mantle plumes tap long-lived reservoirs somewhere in the deep mantle.	Isotopic ratios differ among hotspots; reconciling this may involve multiple reservoirs and/or chemical heterogeneity within thermochemical piles. Entrainment within mantle plumes is expected to be variable, thus hotspot chemistry may vary temporally. Geochemical anomalies do not constrain reservoir depth.
Parallel volcanic tracks at some hotspots	Geochemical observation: parallel tracks of volcanoes with different trace element isotopic ratio behaviour has been noted for several hotspots[37,38].	Plumes preferentially entrain thermochemical pile material from the LLSVP side, and surrounding mantle from the other side of the plume.	How a zoned mantle plume results in parallel volcanic tracks retaining the isotopic signatures from each half of the plume conduit is not well constrained.
CMB topography	Geodynamics prediction: the CMB is upwarped beneath thermochemical piles[60].	Subduction-related downwellings are strong enough to depress the CMB around piles. Thus, the CMB beneath piles is elevated in comparison.	CMB topography predictions depend strongly on density and viscosity differences between piles and surrounding mantle. CMB topography maps from seismology are not in strong agreement.

of LLVPs from thermal properties of lower mantle minerals[46] (for example, reduced wave speeds). A purely thermal origin to present-day LLVPs needs to account for the implied anti-correlation of shear and compressional velocities in places (for example, Supplementary Fig. S4) and the possible presence of post-perovskite in assumed warmer LLVPs. Compositional models have focused on explaining elevated LLVP intrinsic density, which is necessary for long-term dynamic stability, by enrichment of iron. This is a plausible choice, because of the higher mass of Fe than other major elements in the lower mantle[62,63]. However, processes that enrich Fe likely affect the other major element contents, such as Mg, Si, Al, Ca and Na, and therefore mineralogy (Fig. 4). ~~Even simple enrichment of Fe in the lower mantle would result in a greater increase in Fe content in ferropericlase (Fp) than in bridgmanite (Bm) because of strong partitioning of iron into Fp, as long as the Mg/Si ratio remains similar to pyrolite[64,65] (Fig. 4b). Alternatively, a change in partitioning behaviour of Fe (through changes in oxidation or spin state) in the deep mantle could enrich Bm with Fe over Fp. However,~~ possibilities for such change have been highly debated in recent years. While the effects of the other major elements on density are expected to be much smaller, they can impact elastic properties[66,67].

A few models have proposed early formation of the thermochemical piles through fractional crystallization and melting. Crystallization from the mid-lower mantle and the remnant underlying lowermost mantle dense melts may result in structures in the lowermost mantle[51]. Another hypothesis is that dense melt could be trapped in the lowermost upper mantle and sink to the CMB after crystallization[52]. Fe preferentially partitions into melt, and in these

models the partitioning into melt is sufficient enough to make melt either neutrally or negatively buoyant. Although an abrupt change in partitioning of Fe into melt over mineral phases has been suggested at a depth of approximately 2,000 km (ref. 68), more recent studies have questioned this observation[69,70]. Also, it is not fully understood how the fractional melting and crystallization will affect contents of other major elements, such as Mg, Si, Al, Ca and Na, and therefore mineralogy of the structures of the former melts. The impact could be not only changes in the proportion of individual mineral phases but also the appearance of new minerals and disappearance of existing minerals. For example, Na stabilizes the Ca-ferrite-type phase in basalt in the lower mantle[71], but is absent (or only nominally present) in pyrolite (Fig. 4b).

In contrast, LLVPs may have been formed by processes that occurred later than early differentiation. Owing to higher density in the lower mantle[17,67], basaltic material might accumulate and form structures similar to LLVPs[21]. However, if LLVPs were formed purely from basaltic crust, unrealistically high temperatures would be required to explain their shear wave reduction[72]. Alternatively, combined Fe and Si (therefore Bm) enrichment to normal mantle has been shown to provide shear and bulk sound velocity anomalies consistent with LLVPs[73].

If LLVPs were formed through early Earth processes, possibilities exist that might alter the composition through time. Chemical diffusion in the lower mantle is expected to only be a few metres over a timescale of a billion years[74]. However, ongoing deep subduction of basaltic crust can continuously add to existing thermochemical piles[49]. If piles have sufficiently high temperature (~3,500 K), the incorporated basalt may undergo partial melting[75] and react with the pile material. Volatiles can further decrease the melting temperature of basalt. From recent melting experiments and their compositional differences, it can be inferred that the solidus temperature of pyrolite can decrease by as much as 500 K with a few hundred ppm of water at the CMB[69,76,77]. However, the magnitude of the melting temperature decrease remains highly uncertain due to differences in experimental methodologies in existing studies. Recent discoveries of hydrous mineral phases stable at deep mantle conditions[78–81] open up possibilities of deep-water transport. Possible release of water in warm regions of the lowermost mantle can further facilitate metasomatism in thermochemical piles. If chemical reaction between pyrolitic and basaltic materials is significant, then Si and Ca from basalt can increase the fractions of silicate perovskites (Bm and Ca-perovskite) in reaction products by consuming Fp if available (Fig. 4b). While not uniquely constrained, probabilistic tomography favours a 5–10% enrichment in bridgmanite[26,82]. At present, there are no quantitative constraints on the amount of water (for example, phase H minerals) in the lowermost mantle. The role of carbon in the lower mantle[83,84] may also be important for the evolution of deep mantle chemistry, but is similarly unconstrained, as are precise mechanisms for transportation of volatiles to the deep mantle.

Earlier studies[55,56] suggested depletion of Fe in silicate minerals and formation of an Fe–Si alloy through chemical reaction between mantle minerals and the liquid iron of the outer core. While the proposed reaction products have not been found in later studies[85], recent experiments have shown that the lowermost mantle may be depleted in FeO due to the loss to the oxygen-undersaturated outer core[85–88]. Addition of oxygen to the core could have been provided by an oxidized lower mantle basal magma ocean early in Earth's history[88]. Therefore, if Fe loss to the core has been severe, the process may not explain the proposed Fe enrichment in LLVPs unless the Fe–Si alloy reaction product can be incorporated into mantle flow and efficiently accumulate in some manner[89]. Alternatively, liquid Fe might migrate to the mantle due to the chemical gradient caused by the suggested FeO depletion in the lowermost mantle, but such a process might not build structures taller than 100 km (ref. 90). A further uncertainty arises from the possible transport of volatiles, such as water and carbon, which may impact the chemical interaction between the lowermost mantle and the core[80]. Another possibility includes core material percolating into the mantle where slabs depress the CMB[91], creating localized regions of higher density.

The composition of basaltic crust has changed — ancient basalt should be much more MgO-rich than present-day basalt[92], and it is of interest if those earlier basalts were transported to the lowermost mantle. The amount and composition of volatiles transported to the deep interior may have also changed. If such influx of volatiles and recycled materials differ between the CMB regions beneath the Atlantic and Pacific, compositional difference between the two LLVPs cannot be ruled out.

Deep-mantle reservoirs

A deep mantle reservoir that does not actively mix into the mantle (to prevent isotopic signatures characteristic of ocean island basalts, OIBs, from manifesting at mid-ocean ridges) has long been inferred from geochemical analyses of hotspot basalts[93]. Some analyses of isotopic ratios indicate that a deep mantle reservoir may have been in place as early as 80 million years into Earth's history[94] and has been preserved since then. Primordial thermochemical piles are a viable mechanism to explain the unique source for OIB. Numerical simulations demonstrate that plumes can entrain dense pile material, producing estimates of helium ratios (^{3}He/^{4}He) that are quantitatively consistent with OIB geochemistry[72]. Strong seismic heterogeneity is observed within the LLSVPs (Supplementary Fig. S1), and thermal and compositional heterogeneity is predicted by geodynamic models to exist within the piles (Supplementary Fig. S6), especially with the episodic addition of deeply subducted, dense[95] ocean crust[19]. This heterogeneity, combined with variable plume entrainment efficacy[96], suggests a single thermochemical pile can produce a wide range of trace element chemistries in temporally varying, as well as spatially different, plumes that tap it. The possibility that each LLVP may be composed of multiple, smaller parts has also been raised[2,5].

LLVPs relate to fundamental questions about deep mantle convection and the thermal and chemical evolution of the planet. Table 1 summarizes existing seismic observations and interpretations of LLVPs. The thermochemical pile hypothesis can explain the seismically abrupt sides and tops to these regions, the geographical locations of hotspots and LIPs, and isotopic ratio analyses of hotspot lavas (and possibly geochemical zoning in hotspot lavas).

That compositionally distinct LLVPs exist at the base of the mantle today suggests that they have elevated intrinsic density compared with the rock they displace (even though the surrounding mantle may possess high density due to the effect of cooler temperature). If stable today, such large-scale anomalies are likely long-lived, though the precise extent of their longevity is not well constrained. Enhanced Fe content in deep mantle minerals is appealing to explain the observations of increased intrinsic density and seismic velocity reduction of the LLVPs, but the precise chemistry of these compositionally distinct piles depends on unknown factors, especially Earth evolution models, which are not constrained.

Received 16 November 2015; accepted 5 May 2016; published online 20 June 2016

References

1. Ritsema, J., Deuss, A., van Heijst, H. J. & Woodhouse, J. H. S40RTS: a degree-40 shear-velocity model for the mantle from new Rayleigh wave dispersion, teleseismic traveltime and normal-mode splitting function measurements. *Geophys. J. Int.* **184,** 1223–1236 (2011).
2. Lekic, V., Cottaar, S., Dziewonski, A. & Romanowicz, B. Cluster analysis of global lower mantle tomography: a new class of structure and implications for chemical heterogeneity. *Earth Planet. Sci. Lett.* **357,** 68–77 (2012).
3. Garnero, E. J. & McNamara, A. K. Structure and dynamics of Earth's lower mantle. *Science* **320,** 626–628 (2008).

4. Koelemeijer, P., Ritsema, J., Deuss, A. & van Heijst, H. J. SP12RTS: a degree-12 model of shear- and compressional-wave velocity for Earth's mantle. *Geophys. J. Int.* **204,** 1024–1036 (2016).
5. He, Y. & Wen, L. Geographic boundary of the "Pacific Anomaly" and its geometry and transitional structure in the north. *J. Geophys. Res.* **117,** B09308 (2012).
6. Tanaka, S. *et al.* On the vertical extent of the large low shear velocity province beneath the South Pacific Superswell. *Geophys. Res. Lett.* **36,** L07305 (2009).
7. Suetsugu, D. *et al.* South Pacific mantle plumes imaged by seismic observation on islands and seafloor. *Geochem. Geophys. Geosyst.* **10,** Q11014 (2009).
8. French, S. W. & Romanowicz, B. Broad plumes rooted at the base of the Earth's mantle beneath major hotspots. *Nature* **525,** 95–99 (2015).
9. Zhao, C., Garnero, E. J., McNamara, A. K., Schmerr, N. & Carlson, R. W. Seismic evidence for a chemically distinct thermochemical reservoir in Earth's deep mantle beneath Hawaii. *Earth Planet. Sci. Lett.* **426,** 143–153 (2015).
10. Sun, D. & Miller, M. S. Study of the western edge of the African large low shear velocity province. *Geochem. Geophys. Geosyst.* **14,** 3109–3125 (2013).
11. Frost, D. A. & Rost, S. The P-wave boundary of the large-low shear velocity province beneath the Pacific. *Earth Planet. Sci. Lett.* **403,** 380–392 (2014).
12. McNamara, A. K., Garnero, E. J. & Rost, S. Tracking deep mantle reservoirs with ultra low velocity zones. *Earth Planet. Sci. Lett.* **299,** 1–9 (2010).
13. Rost, S., Earle, P. S., Shearer, P. M., Frost, D. A. & Selby, N. D. in *The Earth's Heterogeneous Mantle: A Geophysical, Geodynamical, and Geochemical Perspective* (eds Khan, A. & Deschamps, F.) 367–390 (Springer Publishing, 2015).
14. Frost, D. A., Rost, S., Selby, N. D. & Stuart, G. W. Detection of a tall ridge at the core–mantle boundary from scattered PKP energy. *Geophys. J. Int.* **195,** 558–574 (2013).
15. Cobden, L. & Thomas, C. The origin of D" reflections: a systematic study of seismic array data sets. *Geophys. J. Int.* **194,** 1091–1118 (2013).
16. Cobden, L., Thomas, C. & Trampert, J. *The Earth's Heterogeneous Mantle: A Geophysical, Geodynamical, and Geochemical Perspective* (eds Khan, A. & Deschamps, F.) 391–440 (Springer Publishing, 2015).
17. Nakagawa, T. & Tackley, P. J. Effects of low-viscosity post-perovskite on thermo-chemical mantle convection in a 3-D spherical shell. *Geophys. Res. Lett.* **38,** L04309 (2011).
18. Lay, T., Hernlund, J., Garnero, E. J. & Thorne, M. S. A post-perovskite lens and D" heat flux beneath the Central Pacific. *Science* **314,** 1272–1276 (2006).
19. Li, M., McNamara, A. K. & Garnero, E. J. Chemical complexity of hotspots caused by cycling oceanic crust through mantle reservoirs. *Nature Geosci.* **7,** 336–370 (2014).
20. Brandenburg, J. P. & van Keken, P. E. Deep storage of oceanic crust in a vigorously convecting mantle. *J. Geophys. Res.* **112,** B06403 (2007).
21. Nakagawa, T., Tackley, P. J., Deschamps, F. & Connolly, J. A. D. The influence of MORB and harzburgite composition on thermo-chemical mantle convection in a 3-D spherical shell with self-consistently calculated mineral physics. *Earth Planet. Sci. Lett.* **296,** 403–412 (2010).
22. Grocholski, B., Catalli, K., Shim, S.-H. & Prakapenka, V. B. Mineralogical effects on the detectability of the post-perovskite boundary. *Proc. Natl. Acad. Sci. USA* **109,** 2275–2279 (2012).
23. Grocholski, B., Shim, S.-H. & Prakapenka, V. B. Stability, metastability, and elastic properties of a dense silica polymorph, seifertite. *J. Geophys. Res.* **118,** B50360 (2013).
24. Wang, Y. & Wen, L. Complex seismic anisotropy at the border of a very low velocity province at the base of the Earth's mantle. *J. Geophys. Res.* **112,** B09305 (2007).
25. Lynner, C. & Long, M. D. Lowermost mantle anisotropy and deformation along the boundary of the African LLSVP. *Geophys. Res. Lett.* **41,** 3447–3454 (2014).
26. Trampert, J., Deschamps, F., Resovsky, J. & Yuen, D. A. Probabilistic tomography maps chemical heterogenities throughout the mantle. *Science* **306,** 853–856 (2004).
27. Kuo, C. & Romanowicz, B. On the resolution of density anomalies in the Earth's mantle using spectral fitting of normal-mode data. *Geophys. J. Int.* **150,** 1620179 (2002).
28. Masters, G. & Gubbins, D. On the resolution of density within the Earth. *Phys. Earth Planet. In.* **140,** 159–167 (2003).
29. Romanowicz, B. Can we resolve 3D density heterogeneity in the lower mantle? *Geophys. Res. Lett.* **28,** 1107–1110 (2001).
30. Masters, G., Laske, G., Bolton, H. & Dziewonski, A. M. in *Earth's Deep Interior* (eds Karato, S. *et al.*) 63–87 (Geophysical Monograph Series Vol. 117, American Geophysical Union, 2000).
31. Koelemeijer, P., Duess, A. F., Ritsema, J. & van Heijst, H. J. Normal mode insights into the long wavelength velocity and density structure of the lowermost mantle. Abstr. DI33B-02 (American Geophysical Union, Fall Meeting, 2014).
32. Burke, K., Steinberger, B., Torsvik, T. H. & Smethurst, M. A. Plume generation zones at the margins of large low shear velocity provinces on the core–mantle boundary. *Earth Planet. Sci. Lett.* **265,** 49–60 (2008).
33. Thorne, M., Garnero, E. J. & Grand, S. P. Geographic correlation between hot spots and deep mantle lateral shear-wave velocity gradients. *Phys. Earth Planet. In.* **146,** 47–63 (2004).
34. Torsvik, T. H., Burke, K., Steinberger, B., Webb, S. J. & Ashwal, L. D. Diamonds sampled by plumes from the core–mantle boundary. *Nature* **466,** 352–355 (2010).
35. Davies, D. R., Goes, S. & Sambridge, M. On the relationship between volcanic hotspot locations, the reconstructed eruption sites of large igneous provinces and deep mantle seismic structure. *Earth Planet. Sci. Lett.* **411,** 121–130 (2015).
36. Steinberger, B. & Torsvik, T. H. A geodynamic model of plumes from the margins of large low shear velocity provinces. *Geochem. Geophys. Geosyst.* **13,** Q01W09 (2012).
37. Weis, D., Garcia, M. O., Rhodes, J. M., Jellinek, M. & Scoates, J. S. Role of the deep mantle in generating the compositional asymmetry of the Hawaiian mantle plume. *Nature Geosci.* **4,** 831–838 (2011).
38. Payne, J. A., Jackson, M. G. & Hall, P. S. Parallel volcano trends and geochemical asymmetry of the Society Islands hotspot track. *Geology* **41,** 19–22 (2013).
39. Farnetani, C. G., Hofmann, A. W. & Class, C. How double volcanic chains sample geochemical anomalies from the lowermost mantle. *Earth Planet. Sci. Lett.* **359,** 240–247 (2012).
40. McNamara, A. K. & Zhong, S. Thermochemical piles under Africa and the Pacific. *Nature* **437,** 1136–1139 (2005).
41. Bull, A. L., McNamara, A. K. & Ritsema, J. Synthetic tomography of plume clusters and thermochemical piles. *Earth Planet. Sci. Lett.* **278,** 152–162 (2009).
42. Zhang, N., Zhong, S., Leng, W. & Li, Z. X. A model for the evolution of the Earth's mantle structure since the Early Paleozoic. *J. Geophys. Res.* **115,** B06401 (2010).
43. Thompson, P. F. & Tackley, P. J. Generation of mega-plumes from the core–mantle boundary in a compressible mantle with temperature-dependent viscosity. *Geophys. Res. Lett.* **25,** 1999–2002 (1998).
44. Schubert, G., Masters, G., Olson, P. & Tackley, P. J. Superplumes or plume clusters? *Phys. Earth Planet. In.* **146,** 147–162 (2004).
45. Schuberth, B. S. A., Bunge, H.-P. & Ritsema, J. Tomographic filtering of high-resolution mantle circulation models: Can seismic heterogeneity be explained by temperature alone? *Geochem. Geophys. Geosyst.* **10,** Q05W03 (2009).
46. Davies, D. R., Goes, S., Schuberth, B. S. A., Bunge, H. P. & Ritsema, J. Reconciling dynamic and seismic models of Earth's lower mantle: the dominant role of thermal heterogeneity. *Earth Planet. Sci. Lett.* **353,** 253–269 (2012).
47. Tackley, P. J. in *The Core–Mantle Boundary Region* (eds Gurnis, M. *et al.*) 231–253 (Geodynamic Series, American Geophysical Union, 1998).
48. Nakagawa, T., Tackley, P. J., Deschamps, F. & Connolly, J. A. D. Incorporating self-consistently calculated mineral physics into thermochemical mantle convection simulations in a 3-D spherical shell and its influence on seismic anomalies in Earth's mantle. *Geochem. Geophys. Geosyst.* **10,** Q03004 (2009).
49. Mulyukova, E., Steinberger, B., Dabrowski, M. & Sobolev, S. V. Survival of LLSVPs for billions of years in a vigorously convecting mantle: replenishment and destruction of chemical anomaly. *J. Geophys. Res.* **120,** 3824–3847 (2015).
50. Tolstikhin, I. N., Kramers, J. D. & Hofmann, A. W. A chemical Earth model with whole mantle convection: the importance of a core–mantle boundary layer (D") and its early formation. *Chem. Geol.* **226,** 79–99 (2006).
51. Labrosse, S., Hernlund, J. W. & Coltice, N. A crystallizing dense magma ocean at the base of the Earth's mantle. *Nature* **450,** 866–869 (2007).
52. Lee, C. T. A. *et al.* Upside-down differentiation and generation of a 'primordial' lower mantle. *Nature* **463,** 930–933 (2010).
53. Carlson, R. W. *et al.* How did early Earth become our modern world? *Ann. Rev. Earth Planet. Sci.* **42,** 151–178 (2014).
54. Hirose, K., Fei, Y. W., Ma, Y. Z. & Mao, H. K. The fate of subducted basaltic crust in the Earth's lower mantle. *Nature* **397,** 53–56 (1999).
55. Knittle, E. & Jeanloz, R. Simulating the core–mantle boundary: an experimental study of high-pressure reactions between silicates and liquid iron. *Geophys. Res. Lett.* **16,** 609–612 (1989).
56. Dubrovinsky, L. *et al.* Iron-silica interaction at extreme conditions and the electrically conducting layer at the base of Earth's mantle. *Nature* **422,** 58–61 (2003).
57. Li, M. & McNamara, A. K. The difficulty for subducted oceanic crust to accumulate in upwelling mantle plume regions. *J. Geophys. Res.* **118,** 1–10 (2013).
58. Davaille, A., Girard, F. & Le Bars, M. How to anchor hotspots in a convecting mantle? *Earth Planet. Sci. Lett.* **203,** 621–634 (2002).
59. Tan, E. & Gurnis, M. Compressible thermochemical convection and application to lower mantle structures. *J. Geophys. Res.* **112,** B06304 (2007).
60. Lassak, T. M., McNamara, A. K., Garnero, E. J. & Zhong, S. Core–mantle boundary topography and mantle dynamics. *Earth Planet. Sci. Lett.* **289,** 232–241 (2010).

61. Soldati, G., Koelemeijer, P., Boschi, L. & Deuss, A. Constraints on core–mantle boundary topography from normal mode splitting. *Geochem. Geophys. Geosyst.* **14,** 1333–1342 (2013).
62. Lundin, S. *et al.* Effect of Fe on the equation of state of mantle silicate perovskite over 1 Mbar. *Phys. Earth Planet. In.* **168,** 97–102 (2008).
63. Fei, Y. *et al.* Spin transition and equation of state of (Mg, Fe)O solid solution. *Geophys. Res. Lett.* **34,** L17307 (2007).
64. Irifune, T. *et al.* Iron partitioning and density changes of pyrolite in Earth's lower mantle. *Science* **327,** 193–195 (2010).
65. Nakajima, Y., Frost, D. J. & Rubie, D. C. Ferrous iron partitioning between magnesium silicate perovskite and ferropericlase and the composition of perovskite in the Earth's lower mantle. *J. Geophys. Res.* **117,** B08201 (2012).
66. Jackson, J. M., Zhang, J. Z. & Bass, J. D. Sound velocities and elasticity of aluminous $MgSiO_3$ perovskite: implications for aluminum heterogeneity in Earth's lower mantle. *Geophys. Res. Lett.* **31,** L10614 (2004).
67. Kawai, K. & Tsuchiya, T. Small shear modulus of cubic $CaSiO_3$ perovskite. *Geophys. Res. Lett.* **42,** 2718–2726 (2015).
68. Nomura, R. *et al.* Spin crossover and iron-rich silicate melt in the Earth's deep mantle. *Nature* **473,** 199–202 (2011).
69. Andrault, D. *et al.* Solid-liquid iron partitioning in Earth's deep mantle. *Nature* **487,** 354–357 (2012).
70. Gu, C. *et al.* Electronic structure of iron in magnesium silicate glasses at high pressure. *Geophys. Res. Lett.* **39,** L24304 (2012).
71. Kesson, S. E., Fitz Gerald, J. D. & Shelley, J. M. G. Mineral chemistry and density of subducted basaltic crust at lower-mantle pressures. *Nature* **372,** 767–769 (1994).
72. Deschamps, F., Kaminski, E. & Tackley, P. J. A deep mantle origin for the primitive signature of ocean island basalt. *Nature Geosci.* **4,** 879–882 (2011).
73. Deschamps, F., Cobden, L. & Tackley, P. J. The primitive nature of large low shear-wave velocity provinces. *Earth Planet. Sci. Lett.* **349–350,** 198–208 (2012).
74. Holzapfel, C., Rubie, D. C., Frost, D. J. & Langenhorst, F. Fe–Mg interdiffusion in (Mg, Fe)SiO_3 perovskite and lower mantle reequilibration. *Science* **309,** 1707–1710 (2005).
75. Andrault, D. *et al.* Melting of subducted basalt at the core–mantle boundary. *Science* **344,** 892–895 (2014).
76. Fiquet, G. *et al.* Melting of peridotite to 140 gigapascals. *Science* **329,** 1516–1518 (2010).
77. Nomura, R. *et al.* Low core–mantle boundary temperature inferred from the solidus of pyrolite. *Science* **343,** 522–525 (2014).
78. Tsuchiya, J. First principles prediction of a new high-pressure phase of dense hydrous magnesium silicates in the lower mantle. *Geophys. Res. Lett.* **40,** 4570–4573 (2013).
79. Nishi, M. *et al.* Stability of hydrous silicate at high pressures and water transport to the deep lower mantle. *Nature Geosci.* **7,** 224–227 (2014).
80. Ohira, I. *et al.* Stability of a hydrous δ-phase, AlOOH-$MgSiO_2(OH)_2$, and a mechanism for water transport into the base of lower mantle. *Earth Planet. Sci. Lett.* **401,** 21–27 (2014).
81. Ohtani, E., Amaike, Y., Kamada, S., Sakamaki, T. & Hirao, N. Stability of hydrous phase H $MgSiO_4H_2$ under lower mantle conditions. *Geophys. Res. Lett.* **41,** 8283–8287 (2014).
82. Mosca, I., Cobden, L., Deuss, A., Ritsema, J. & Trampert, J. Seismic and mineralogical structures of the lower mantle from probabilistic tomography. *J. Geophys. Res.* **117,** B06304 (2012).
83. Seto, Y., Hamane, D., Nagai, T. & Fujino, K. Fate of carbonates within oceanic plates subducted to the lower mantle, and a possible mechanism of diamond formation. *Phys. Chem. Miner.* **35,** 223–229 (2008).
84. Oganov., A. R., Ono, S., Ma, Y., Glass, C. W. & Garcia, A. Novel high-pressure structures of $MgCO_3$, $CaCO_3$, and CO_2 and their role in Earth's lower mantle. *Earth Planet. Sci. Lett.* **273,** 38–47 (2008).
85. Takafuji, N., Hirose, K., Mitome, M. & Bando, Y. Solubilities of O and Si in liquid iron equilibrium with (Mg, Fe)SiO_3 perovskite and the light elements in the core. *Geophys. Res. Lett.* **32,** L06313 (2005).
86. Ozawa, H. *et al.* Chemical equilibrium between ferropericlase and molten iron to 134 GPa and implications for iron content at the bottom of the mantle. *Geophys. Res. Lett.* **35,** L05308 (2008).
87. Frost, D. J. *et al.* Partitioning of oxygen between the Earth's mantle and core. *J. Geophys. Res.* **115,** B02202 (2010).
88. Badro, J., Côté, A. S. & Brodholt, J. P. A seismologically consistent compositional model of Earth's core. *Proc. Natl. Acad. Sci. USA* **111,** 7542–7545 (2015).
89. Manga, M. & Jeanloz, R. Implications of a metal-bearing chemical boundary layer in D" for mantle dynamics. *Geophys. Res. Lett.* **23,** 3091–3094 (1996).
90. Otsuka, K. & Karato, S.-I. Deep penetration of molten iron into the mantle caused by a morphological instability. *Nature* **492,** 243–246 (2012).
91. Kanda, R. V. S. & Stevenson, D. J. Suction mechanism for iron entrainment into the lower mantle. *Geophys. Res. Lett.* **33,** L02310 (2006).
92. Johnson, T. E., Brown, M., Kaus, B. J. P. & VanTongeren, J. A. Delamination and recycling of Archaean crust caused by gravitational instabilities. *Nature Geosci.* **7,** 47–52 (2013).
93. Hofmann, A. W. & S. R. Hart. Assessment of local and regional isotopic equilibrium in the mantle. *Earth Planet. Sci. Lett.* **38,** 44–62 (1978).
94. Mukhopadhyay, S. Early differentiation and volatile accretion recorded in deep-mantle neon and xenon. *Nature* **486,** 101–104 (2012).
95. Ricolleau, A. *et al.* Phase relations and equation of state of a natural MORB: implications for the density profile of subducted oceanic crust in the Earth's lower mantle. *J. Geophys. Res.* **115,** B08202 (2012).
96. Williams, C. D., Li, M., McNamara, A. K., Garnero, E. J. & van Soest, M. C. Episodic entrainment of deep primordial mantle material into ocean island basalts. *Nature Commun.* **6,** 8937 (2015).
97. McDonough, W. F. & Sun, S.-S. The composition of the Earth. *Chem. Geol.* **120,** 223–253 (1995).
98. Schilling, J.-G. *et al.* Petrologic and geochemical variations along the mid-Atlantic ridge from 29°N to 73°N. *Am. J. Sci.* **283,** 510–586 (1983).
99. Kesson, S. E., Fitz Gerald, J. D. & Shelley, J. M. Mineralogy and dynamics of a pyrolite lower mantle. *Nature* **393,** 252–255 (1998).
100. Hirose, K., Takafuji, N., Sata, N. & Ohishi, Y. Phase transition and density of subducted MORB crust in the lower mantle. *Earth Planet. Sci. Lett.* **237,** 239–251 (2005).

Acknowledgements

The authors thank T. Torsvik for the LIP and kimberlite data set, seismic tomographers that made their models publically available, D.A. Frost and P. Koelemeijer for fruitful discussions, and J. Ritsema, F. Deschamps and A. Stracke for abundant helpful comments. M. Li provided model results and images from ref. 19 that were the basis of Supplementary Fig. S6. This research was partially supported by National Science Foundation grants EAR1401270, EAR1161038 and EAR1338810.

Author contributions

E.J.G., A.K.M., and S.-H.S. equally contributed to the text. E.J.G. constructed the figures with active involvement from A.K.M. and S.-H.S.

Additional information

Reprints and permissions information is available online at www.nature.com/reprints. Correspondence and requests for materials should be addressed to E.J.G.

Competing financial interests

The authors declare no competing financial interests.

nature geoscience

SUPPLEMENTARY INFORMATION

DOI: 10.1038/NGEO2733

Continent-sized anomalous zones with low seismic velocity at the base of Earth's mantle

Edward J. Garnero[1], Allen K. McNamara[1], and Sang-Heon D. Shim[1]

[1]School of Earth and Space Exploration, Arizona State University, Tempe AZ, USA 85287-6004

In this paper, we discuss large low velocity provinces (LLVPs) in Earth's lowermost mantle, explore their dynamics and possible composition, and consider evolutionary scenarios. The question of thermochemical piles as the origin to LLVPs is important, as it forms the foundation for our understanding of the thermal state of the mantle, the thermal and chemical evolution of Earth's interior, the dynamics and geochemical significance of mantle plumes, and link to the driving forces causing plate tectonics. This supplementary material presents additional figures to support discussions presented in the main text.

Supplementary Figure S1 presents a number of tomography models, and compares details of LLSVPs, in particular, for 30% of the core-mantle boundary's (CMB's) area. For each model, the specific shear velocity reduction which, when a contour is computed, surrounds 30% of the CMB's area, is determined (and listed to the left of the models in Figure S1). The similarity among models of the long wavelength character of LLSVPs is striking. However, when scale lengths smaller than LLSVP dimensions are considered, significant variability (differences) among models is present (right column, Figure S1). This is not unexpected, given that different models use different methods and data. Resolution from region to region is typically non-uniform in

the tomographic approach. For example, Earth's southern hemisphere is significantly more poorly sampled[101].

Figure S3 shows the locations where forward modeling studies have mapped strong changes in *Vs* occurring over short lateral distances, such as < 100 km. These are considered "sharp" in comparison to smoothly varying tomographically derived velocities.

We consider a related comparison of the first 8 tomographic models of Figure S1. We compare the lowest shear velocities in each model that occupy a defined percent of the CMB's area, and then we count the number of models having those lowest velocities in 1°×1° cells (Figure S2). When mapping the 10% of the CMB's area containing the lowest velocities in tomography models (top panel in Figure S2), we find that these regions are generally correlated with the interior of 30% area LLSVPs (red contours in Figure S1), with some geographical differences. For greater area percentages of the CMB (e.g., 20, 30, 40, and 50% areas, the other panels in Figure S2), a larger area of similarity between models is present, but differences in the perimeters of the low velocities are readily apparent. These differences are highlighted for the 30% area LLSVPs in Figure 1c (in the main text). The vertical extent of LLSVP low velocities varies from model to model (in both forward and inverse modeling), and depends on assumptions of the velocity value associated with their margins. Though, analyses of the depth distribution of shear velocity heterogeneity (δV_S) over the bottom 1800 km of the mantle (averaged laterally in 4°×4° cells) show strong similarity between models in their geographic distribution of their high-versus-low velocity clusters over that depth range[2].

Lateral gradients in the shear velocity perturbation maps were computed. Gradients were measured by computing the change in shear velocity over different lateral distances (from 3 to 10 degrees, which at the CMB corresponds to ~182 km and ~607 km, respectively). We display the amplitude of the gradient field for 10 degree measurement length in Figure S5. The strongest gradients are most commonly associated with the margins of LLSVPs. This is consistent with abrupt changes in shear velocity at those locations (and the thermochemical pile hypothesis).

A time snapshot from the geodynamic calculations of Li et al. (2014) (ref. 19) is explored in Figure S6. Composition and temperature fields are shown for a calculation with distinct thermochemical pile material, former oceanic crust material, and background mantle material. The zoomed in panels show that crust can enter the piles and add to compositional complexities, and that the temperature variability within thermochemical piles can be strong, which might be an explanation for observed seismic heterogeneity within LLSVPs. While the details depend strongly on model assumptions, we expect a similar result – that thermal and potentially chemical heterogeneity can persist within thermochemical piles, especially over long time periods.

Additional References

101. Simmons, N. A., Forte, A., Boschi, L. & Grand, S. P. GyPSuM: a joint tomographic model of mantle density and seismic wave speeds. *J. Geophys. Res*. **115**, B12310 (2010).
102. Houser, C., Masters, G., Shearer, P. & Laske, G. Shear and compressional velocity models of the mantle from cluster analysis of long-period waveforms. *Geophys. J. Int*. **174**, 195–212 (2008).
103. Kustowski, B., Ekstrom, G. & Dziewonski, A. M. Anisotropic shear-wave velocity structure of the Earth's mantle: a global model. *J. Geophys. Res*. **113**, B06306 (2008).
104. Mégnin, C., & Romanowicz, B. The shear velocity structure of the mantle from the inversion of body, surface, and higher modes waveforms. *Geophys. J. Int*. **143**, 709–728 (2000).
105. Grand, S. P. Mantle shear wave tomography and the fate of subducted slabs. *Phil. Trans. R. Soc. Lond. A* **360**, 2475-2491 (2002).
106. Becker, T. W. & Boschi, L. A comparison of tomographic and geodynamic mantle models. *Geochem. Geophys. Geosyst*. **3,** 2001GC000168 (2002).
107. Bréger, L. & Romanowicz, B. Thermal and chemical 3D heterogeneity in D". *Science* **282**, 718-720 (1998).
108. Luo, S., Ni, S., & Helmberger, D. V. Evidence for a sharp lateral variation of velocity at the core–mantle boundary from multipathed PKPab. *Earth Planet. Sci. Lett.*, **189**, 155-164 (2001).
109. Ni, S., Tan, E., Gurnis, M. & Helmberger, D. V. Sharp Sides to the African Superplume. *Science* **296**, 1850-1852 (2002).
110. Ni, S. & Helmberger, D. V. Further constraints on the African superplume structure. *Phys. Earth Planet. Int*. **140**, 243-251 (2003).
111. Ni, S. & Helmberger, D. V. Ridge-like lower mantle structure beneath South Africa. *J. Geophys. Res*. **108**, 2094 (2003).
112. Ni, S. & Helmberger, D. V. Seismological constraints on the South African superplume: could be the oldest distinct structure on Earth. *Earth Planet. Sci. Lett*. **206**, 119-131 (2003).
113. Ni, S., Helmberger, D. V. & Tromp, J. Three-dimensional structure of the African superplume from waveform modeling. *Geophys. J. Int*. **161**, 283-294 (2005).
114. Wang, Y. & Wen, L. Mapping the geometry and geographic distribution of a very-low velocity province at the base of the Earth's mantle. *J. Geophys. Res*. **109**, B10305 (2004).
115. To, A., Romanowicz, B., Capdeville, Y. & N. Takeuchi. 3D effects of sharp boundaries at the borders of the African and Pacific Superplumes: Observation and modeling. *Earth Planet. Sci. Lett*. **233**, 137-153 (2005).
116. He, Y., Wen, L. & Zheng, T. Geographic boundary and shear wave velocity structure of the "Pacific anomaly" near the core–mantle boundary beneath western Pacific. *Earth Planet. Sci. Lett*. **244**, 302-314 (2006).
117. Ford, S. R., Garnero, E. J. & McNamara, A. K. A strong lateral shear velocity gradient and anisotropy heterogeneity in the lowermost mantle beneath the southern Pacific. *J. Geophys. Res*. **111**, 1-14 (2006).

118. Sun, D., Tan, E., Helmberger, D. V. & M. Gurnis. Seismological support for the metastable superplume model, sharp features, and phase changes within the lower mantle. *Proc. Natl. Acad. Sci*. **104**, 9151-9155 (2007).
119. Sun, D., Helmberger, D. V., Ni, S. & Bower, D. Direct measures of lateral velocity variation in the deep Earth. J. *Geophys. Res*. **114**, 1-18 (2009).
120. He, Y. & Wen, L. Structural features and shear-velocity structure of the "Pacific Anomaly". *J. Geophys. Res*. **114**, B02309 (2009).

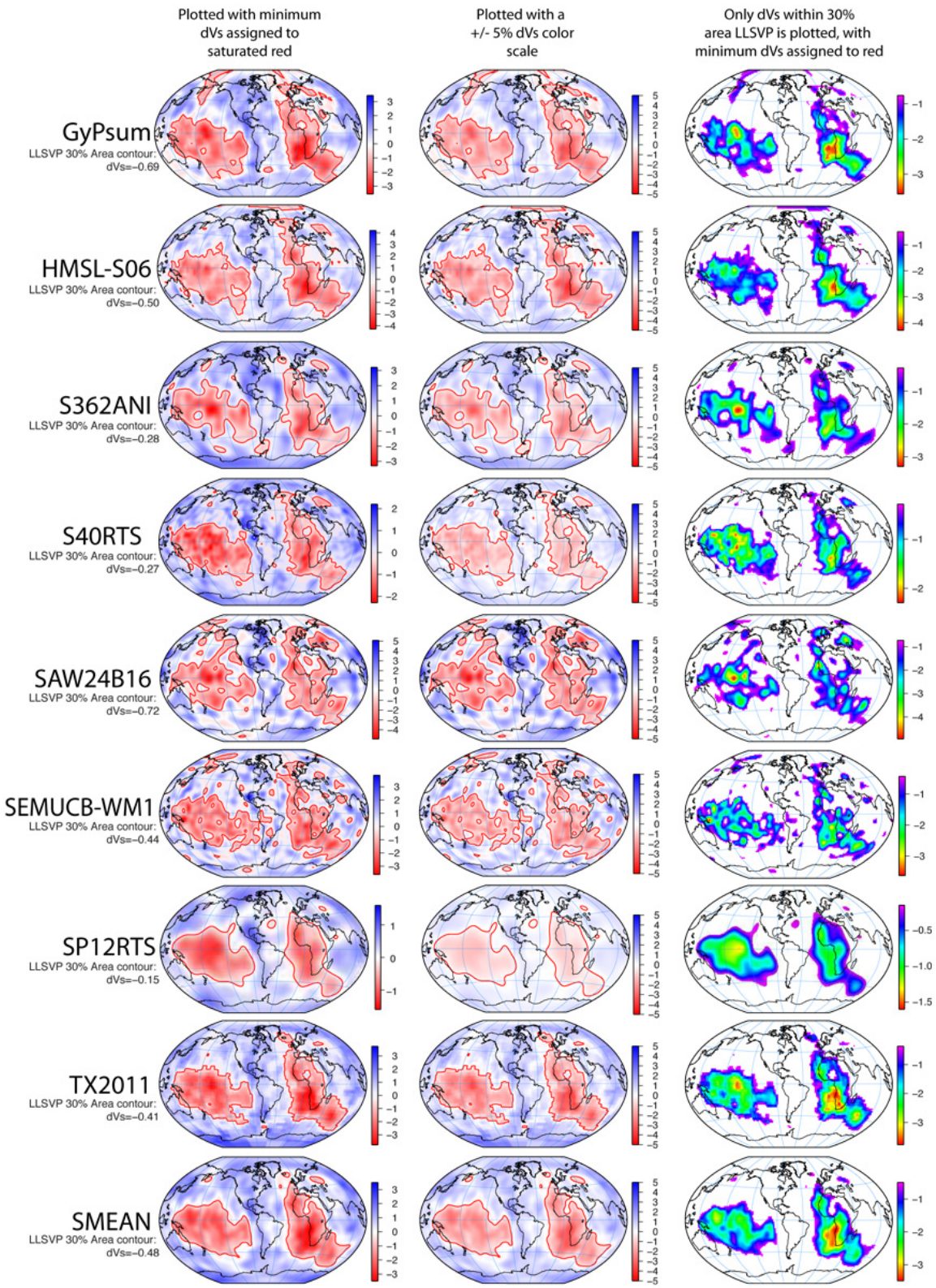

Figure S1 | Comparison of tomography model lowermost mantle velocities. (All scale bars in % δVs). For 8 tomographic models (GyPsum (ref. 101), HML-S06 (ref. 102), S362ANI (ref. 103), S40RTS (ref. 1), SAW24B16 (ref. 104), SEMUCB-WM1 (ref. 8), SP12RTS (ref. 4), TX2011 (ref. 105)), and SMEAN, an average of models (ref. 106), the

lowest 200 km depth in each model is plotted. In the left column, the color scale extremes correspond to each model's extremes in high (blue) and low (red) shear velocity perturbations. A red contour is drawn at a velocity level for each model that surrounds 30% of the CMB containing the lowest shear velocities. Thus, the same CMB area (30%) is contoured for each model. The velocity reduction value that this corresponds to is shown on the left for each model. The middle column is the same as the left column, except the color scales are the same for all model renderings, and set at +/- 5%, to show the amplitude differences between models. In the right column, only the area within the red contours of the left columns is considered (i.e., the 30% area LLSVPs), and the color scale is chosen to highlight shear velocity heterogeneity within LLSVPs for the CMB area coverage (again, 30%). The intermediate and small scale LLSVP heterogeneity differs from model to model.

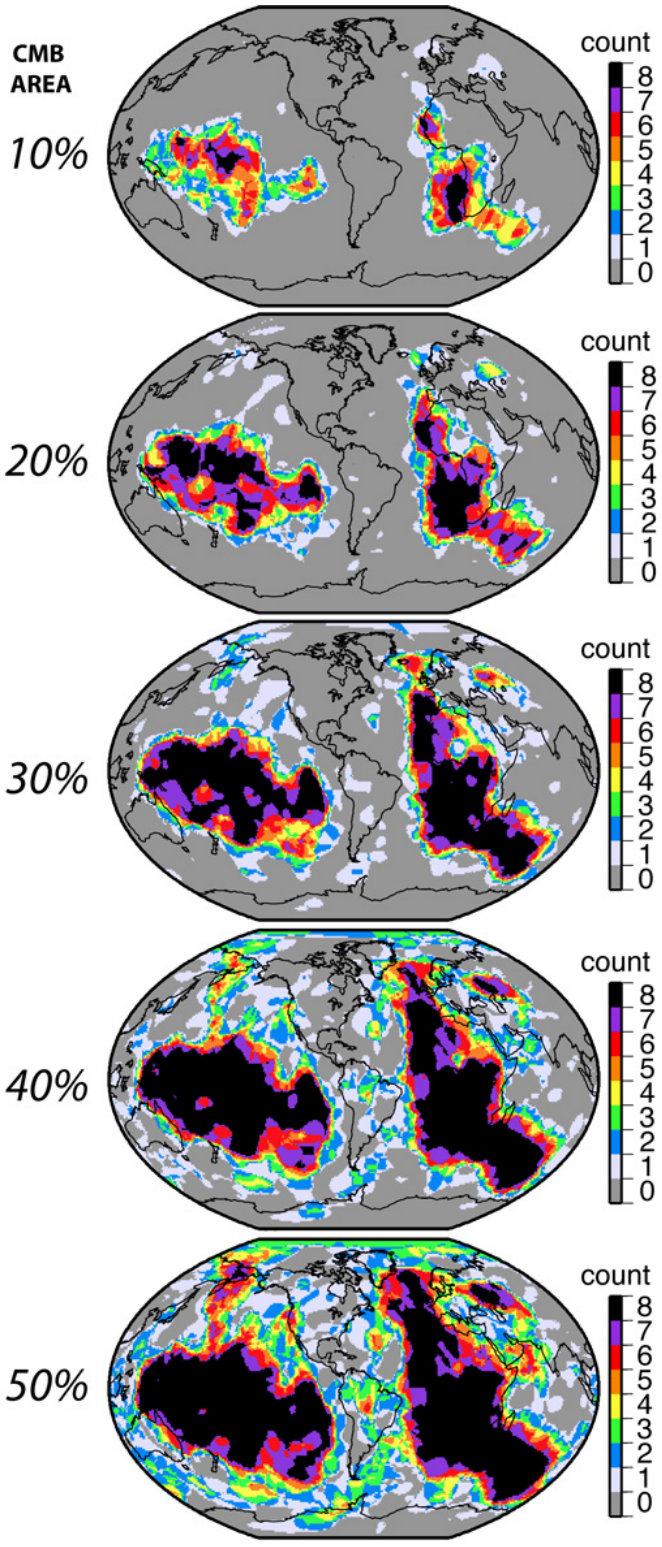

Figure S2 | Comparison of tomography model lowest velocity regions for specific CMB areas of coverage. For the first 8 tomographic models shown in Figure S1, the lowest velocities in each model are considered according to specific percentages of the area of the CMB. The CMB is gridded into 1°×1° cells, and models with lowest velocities

(for given CMB areas of consideration) are counted in all cells, and displayed in “vote maps”. Since 8 models are considered, a black color (as in the color scale) represents an area where all 8 models have some part of their lowest velocities at that location. Conversely, the color gray indicates that no model had its lowest velocities at that location, for the amount of LLSVP area considered. Five lowest velocity areas are considered 10, 20, 30, 40, and 50%.

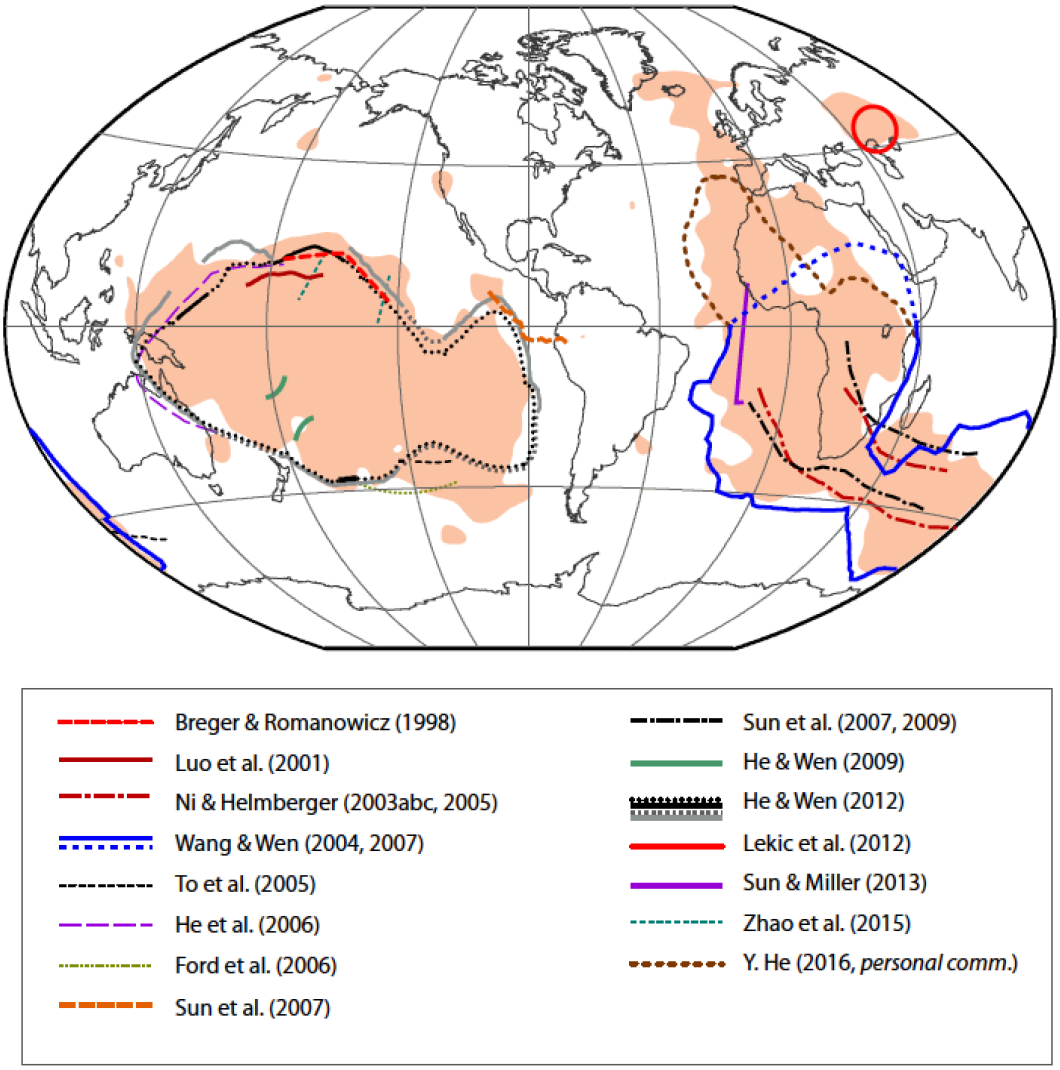

Figure S3 | Locations of sharp LLSVP edges. Waveform and travel time studies have presented evidence for sharp transitions in shear velocity at the margins of LLSVPs. The studies listed are Breger & Romanowicz (1998)[107], Luo et al. (2001)[108], Ni & Helmberger (2003abc) and Ni et al. (2002, 2005)[109-112], Wang & Wen (2004, 2007)[24,114], To et al. (2005)115, He et al. (2006)116, Ford et al. (2006)[117], Sun et al. (2007, 2009)[118,119], He & Wen (2009,2012)[5,120], Lekic et al. (2012)[2], Sun & Miller (2013)[10], Zhao et al. (2015)[9], and Yumei He (2006, personal comm.).

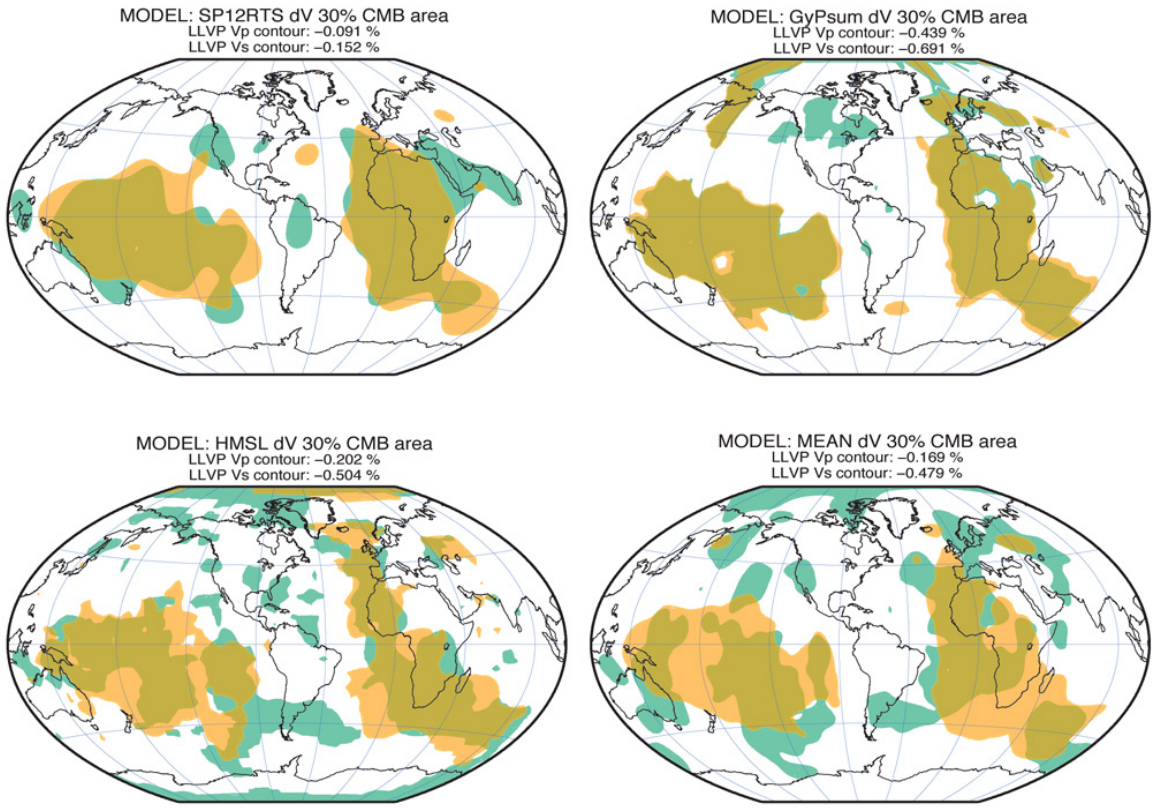

Figure S4 | Comparison of P-wave and S-wave LLVPs. The lowermost mantle velocity reductions for both P-wave (green) and S-wave (orange) LLVPs are displayed for 3 tomography studies that simultaneously inverted for Vp and Vs: SP12RTS (ref. 4), GyPsum (ref. 101), HMSL (ref. 102), and an average of P and S models, from PMEAN and SMEAN (ref. 106). LLVPs that occupy 30% of the CMB's area is displayed.

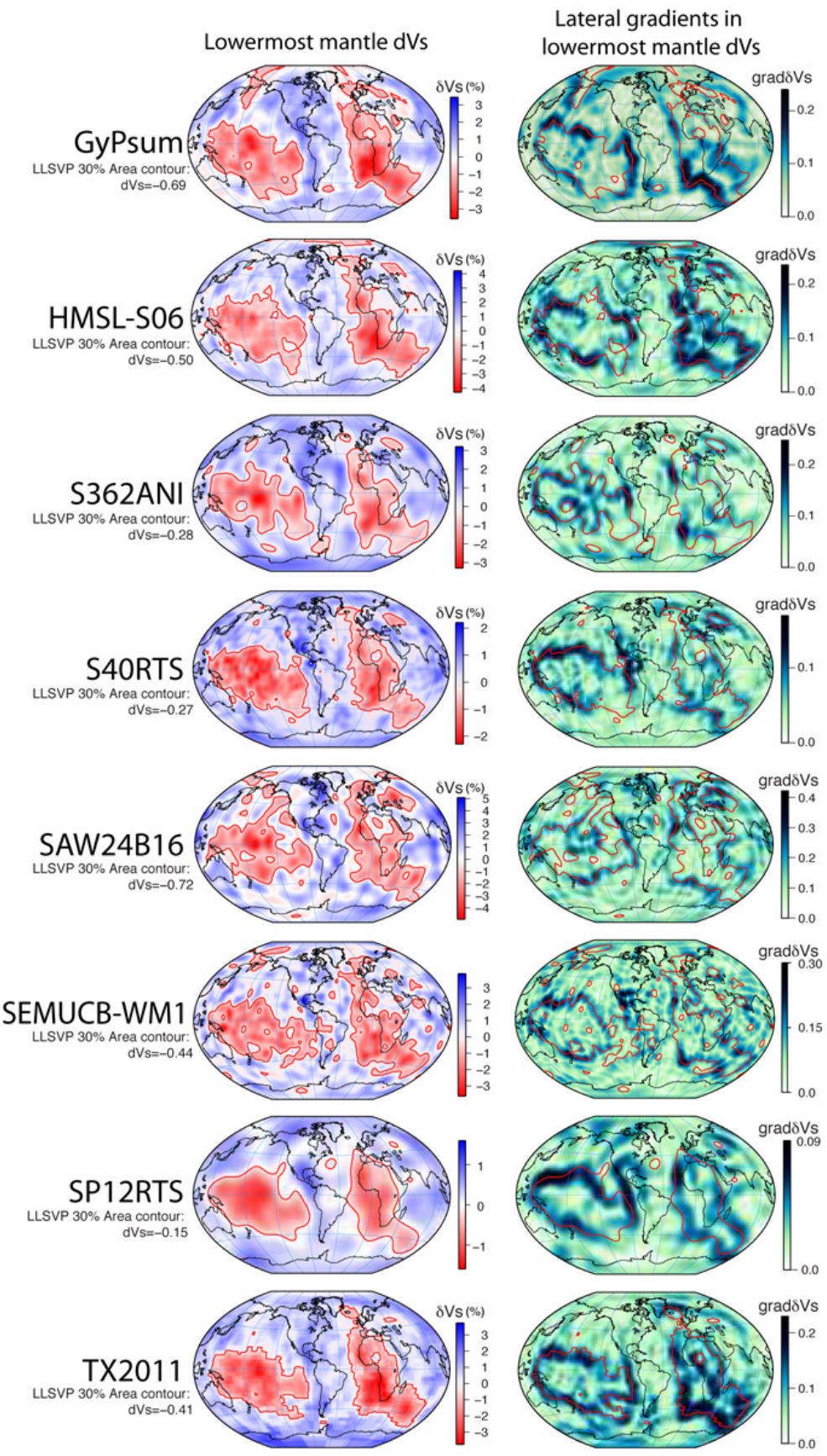

Figure S5 | Comparison of tomography model LLSVPs and strongest lateral gradients (*previous page*). *(Left column)* As with the left column in Figure S1, the shear velocity perturbations are shown in the lowest 200 km of the mantle, for 8 tomography models. The color scale is set for each model's extreme high or low shear velocities. The LLSVP contour is drawn for the 30% CMB area level. *(Right column)* Lateral gradients in the shear velocity perturbation field are plotted, where the darkest colors correspond to strongest gradients. The color scale for each model is different, and set by that model's maximum gradient. The LLSVP contour from the left column is reproduced on the gradient field, and shows the strongest gradients are commonly at the 30% area LLSVP margins. The maximum lateral gradient is computed over a 10 degree lateral length at every 1 deg by 1 deg location, which is plotted.

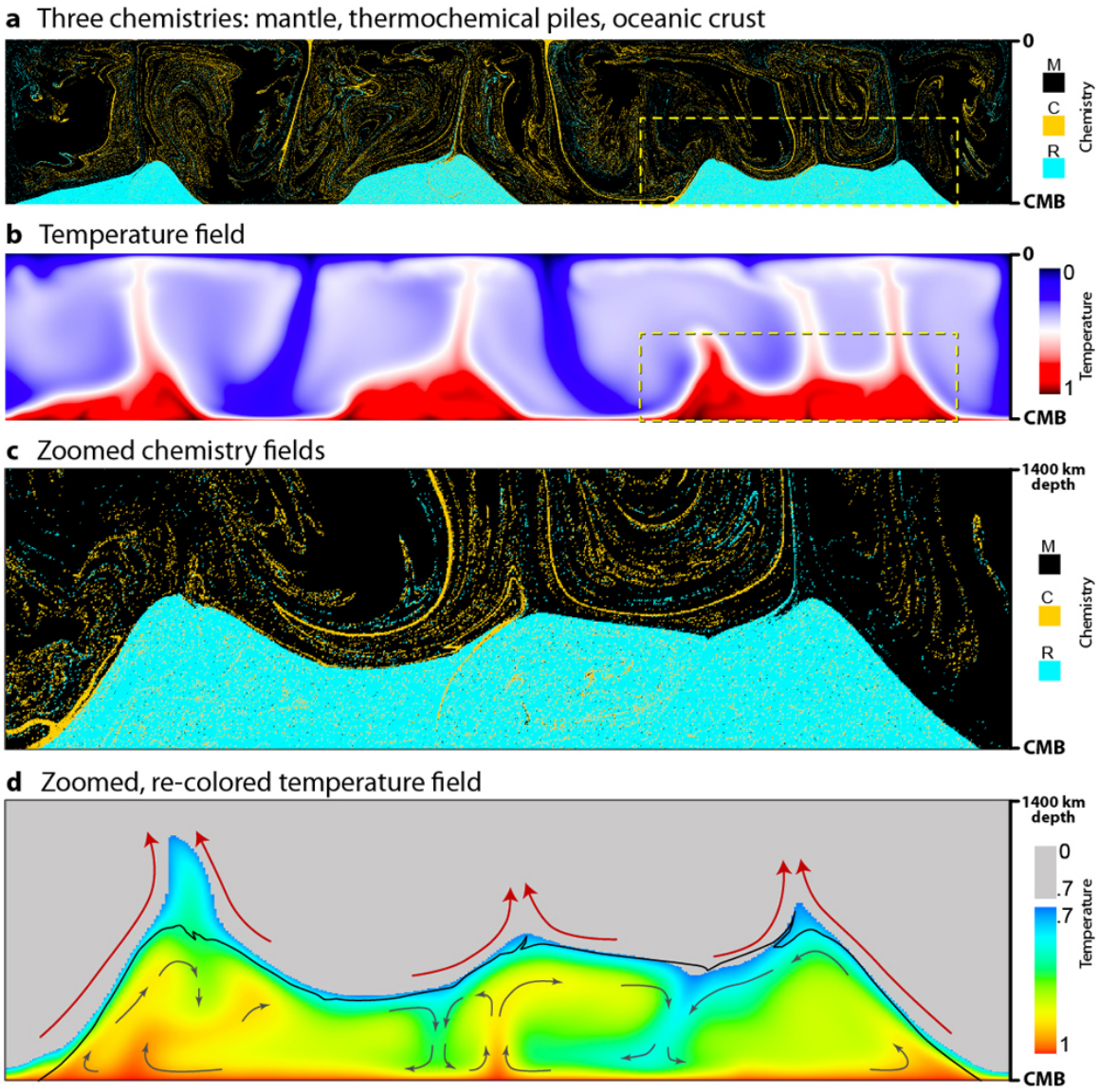

Figure S6 | Predictions of internal structure of thermochemical piles. From the calculations of Li et al. (2014)[19] the dynamics, composition, and temperature are shown for a 3 chemistry system: a thermochemical reservoir at the base of the mantle ("R"), former basaltic oceanic crust ("C"), and background mantle ("M"). **a,** The compositional field is displayed for a time snapshot with thermochemical piles (turquoise color) well developed. Former oceanic crust (yellow color) is well mixed into the mantle (black color is the mantle), and has also been downward entrained into the piles. **b,** The temperature field for the time snapshot of **a** is shown. Panels **c** and **d** correspond to the zoom boxes in **a** and **b,** and show the composition and temperature. The temperature field in **d** is modified to show a complete color scale just within the thermochemical pile to highlight internal convection. The pile margin based on chemistry is indicated by the black line; flow directions are indicated by the arrows. For this example, the temperature field between .7 and 1 is colorized, with the rest plotted as gray.